Assignment of ^{15}N Chemical Shifts and ^{15}N Relaxation Measurements for Oxidized and Reduced Iso-1-cytochrome *c*[†]

Jacquelyn S. Fetrow[‡] and Susan M. Baxter*[,§]

Wadsworth Center and Department of Biomedical Sciences, New York State Department of Health, Empire State Plaza, Albany, New York 12201-0509, and Department of Molecular Biology, The Scripps Research Institute, 10550 North Torrey Pines Drive, La Jolla, California 92037

Received November 18, 1998; Revised Manuscript Received January 27, 1999

ABSTRACT: A protocol for complete isotopic labeling of iso-1-cytochrome *c* from the eukaryote *Saccharomyces cerevisiae* is reported. Assignments are reported for the vast majority of the ^{15}N amide resonances in both oxidized and reduced states. ^{15}N heteronuclear relaxation experiments were collected to study the picosecond−nanosecond backbone dynamics of this protein. Relaxation rates were computed and fit to spectral density functions by a model-free analysis. Backbone amides in the overlapping loop B/C region are the most flexible on the picosecond−nanosecond time scale in both forms of the protein. The results show that, on average, the protein backbone is slightly more dynamic in the oxidized than the reduced state, though not significantly so. Exchange terms, which suggest significant motion on a time scale at least an order of magnitude slower than the overall correlation time of 5.2 ns, were required for only two residues in the reduced state and 27 residues in the oxidized state. When analyzed on a per-residue basis, the lower order parameters found in the oxidized state were scattered throughout the protein, with a few continuous segments found in loop C and the C-terminal helix, suggesting greater flexibility of these regions in the oxidized state. The results provide dynamic interpretations for previously presented structural and functional data, including redox-dependent changes that occur in the protein. The way is now paved for extensive dynamic analysis of variant cytochromes *c*.

Cytochromes *c* are small proteins that function as electron carriers between the last two complexes in the electron transport chain of eukaryotic organisms (*1*). These globular proteins fold around an iron-containing heme group that is responsible for accepting an electron from cytochrome *c* reductase and transferring an electron to cytochrome *c* oxidase. In shuttling electrons between electron donor and acceptor proteins, the iron in the heme group alternates between the reduced, diamagnetic form Fe(II) and the oxidized, paramagnetic form Fe(III). The surrounding protein is responsible for maintaining the redox state of the iron in an aqueous cellular environment and for recognizing and docking to the appropriate redox partners.

Cytochrome *c* from yeast is well-behaved for biophysical and biochemical studies and has been used as a model for studying protein folding and structure/function relationships. High-resolution structures for the oxidized and reduced forms of yeast iso-1-cytochrome *c*, including several mutant forms of the protein, have been determined by X-ray crystallography and NMR spectroscopy (*2*−*7*). The fold of iso-1-cytochrome *c* consists of α helices and loop structures. The polypeptide chain folds into a series of structural elements: N-terminal helix (Ala 3−Arg 13), loop A (His 18−Leu 32), the overlapping loops B (Gly 34−Gly 45) and C (Ser 40−Lys 54), 60s helix (Asp 60−Thr 69), loop D (Asn 70−Gly 84), and the C-terminal helix (Lys 87−Thr 102). The loops of C102T are not unstructured entities; rather they contain regions of approximate α-helical geometry, extended segments, and β-turn structures, forming Ω loops with hydrogen-bonding networks (*8*). The heme group is covalently attached to the polypeptide chain at Cys 14 and Cys 17 by thioether linkages. The heme iron is coordinated by the His 18 (loop A) and Met 80 (loop D) side chains. The overall fold of the protein does not change significantly with redox state (*7*, *9*).

Despite very similar crystallographic and NMR structures for the reduced and oxidized forms of iso-1-cytochrome *c*, several groups (*10*−*13*) have noted a large difference in the folding energetics between the two redox states of the protein. Supporting this observation, differential scanning calorimetry experiments (*11*) have measured a 6−7 kcal mol^{-1} increase in thermal stability upon reduction. To further understand and describe features of the structures related to this difference in stability, hydrogen exchange NMR experiments have been carried out by several groups. Marmorino et al. (*14*) have shown that reduction of the heme group in iso-1-cytochrome *c*, carrying the C102T mutation, results in a generalized slowing of hydrogen exchange rates, implying a general increase in the free energy (ΔG_{op}) for local unfolding. Recently, Banci et al. (*7*) used hydrogen exchange data to propose specifically that the loop A and loop D regions had greater "flexibility" in the oxidized form of iso-

[†] This work was partially supported by NIH Grant GM44829 to J.S.F.

* To whom correspondence should be addressed at Wadsworth Center, New York State Department of Health, Empire State Plaza, P.O. Box 509, Albany, NY 12201-0509; phone 518-486-7320; email baxter@wadsworth.org.

[‡] The Scripps Research Institute.

[§] New York State Department of Health.

10.1021/bi9827417 CCC: $18.00
Published on Web 03/17/1999

1-cytochrome *c*, carrying the C102S mutation, relative to the reduced form.

We have used NMR methods to characterize the dynamics of iso-1-cytochrome *c* (C102T) in an effort to relate them to stability, function, and changes in redox state. The C102T variant has been used in these and in previous biophysical studies because it is structurally and functionally similar to the wild-type protein (*9, 15*) but is better behaved in solution (*16*). As previously reported, we have expressed and purified a [*U*-^{15}N] isotopically labeled C102T sample from yeast and compared the hydrogen exchange behavior of the C-terminal helix in oxidized and reduced forms (*17*). In this work, heteronuclear, multidimensional NMR experiments were used to assign the nitrogen resonances of a majority of the backbone amide ^{15}N chemical shifts in both oxidized and reduced forms of C102T at pH 4.6. The accompanying paper describes hydrogen exchange experiments on C102T to probe the slower (millisecond−second) time scale dynamics of the protein backbone (*18*). In this paper, we describe the effect of the heme iron redox state on backbone dynamics using ^{15}N relaxation measurements, a technique that probes fast (picosecond−nanosecond) time scale motions. Model-free analysis of the ^{15}N relaxation rates suggests that the oxidized protein has greater flexibility on the picosecond−nanosecond time scale relative to the reduced form. In particular, backbone amides in the overlapping loop B/C region are the most flexible on the picosecond−nanosecond time scale in both forms of the protein. Conformational exchange on a slower time scale was identified for a significant number of residues, spread throughout the oxidized protein, further indicating greater flexibility relative to the reduced form of C102T.

MATERIALS AND METHODS

Overexpression and Purification of [U-^{15}N]C102T: (A) Yeast Strains and Proteins. Saccharomyces cerevisiae strain C93 (*19*) produces C102T, the iso-1-cytochrome *c* variant in which the cysteine at position 102 is replaced by threonine. This variation eliminates intermolecular dimerization and thus facilitates in vitro analysis of the protein. Its properties are virtually identical to those of true wild-type iso-1-cytochrome *c* (*9, 20*), and it has been used as the "wild type" by us (*21*) and by other researchers (*14, 15, 22*). Strain C93 does not produce iso-2-cytochrome *c* (*19*). For optimization experiments, a strain containing a complete deletion of the *CYC1* locus, C15 (*19*), was also used. C93d, the diploid of strain C93, was produced by crossing C93 with strain B2111 (*8*).

(B) Growth Curves and Low-Temperature Spectroscopy. Optimization of the medium and growth conditions for production of C102T in minimal medium was performed in 10 mL cultures prepared in sidearm flasks. These cultures were grown with vigorous shaking at 30 °C for 14 h. Culture density was then determined with a Klett−Summersen colorimeter, as previously described (*21*). The amount of holocytochrome *c* present in the cells at the end of incubation was determined by low-temperature difference spectroscopy of the intact yeast cells (*21*). For analysis, the culture density and spectroscopic absorbance were normalized to those quantities determined for C93 grown in YPD (1% yeast extract, 2% Bacto-peptide, and 2% dextrose) medium (100%) and for C15, a strain that produces no cytochrome *c*, grown in YPD (0%).

(C) Yeast Fermentation and Purification of C102T. Final minimal medium composition for production of C102T was 40 mM Bis-Tris (pH 6.5), 6.5 mg/mL yeast nitrogen base (YNB), 20 mg/mL dextrose, 2.0 mg/mL ammonium sulfate, 1.3 mg/mL Celtone, and 40 mL of salt solution (0.25 M K_2HPO_4, 0.25 M KH_2PO_4, 0.1 M $MgSO_4$, 2 mM $MgCl_2$, and 11 μM $FeCl_2$). All components were autoclaved, except the Celtone, which was sterilized through a 0.22 μm filter and added to the autoclaved medium after it cooled. To produce labeled C102T, ^{15}N ammonium sulfate and Celtone-N (Martek) were substituted for the unlabeled components.

For fermentation of a large batch of labeled C102T, an overnight culture was prepared by inoculating 200 mL of minimal medium with freshly prepared C93d. This culture was grown at 30 °C with vigorous shaking for 18−22 h. Five liters of minimal medium was prepared and placed in a 7-L fermentor vessel. Antibiotics (0.1 g/L streptomycin and 0.04 g/L chloramphenicol), 6 mL/L ethanol, and 0.5 mL of Antifoam A were added. This medium was inoculated with the 200 mL overnight culture and the culture was grown for 5 days at 30 °C with vigorous stirring and aeration. Samples of this culture were checked daily for culture turbidity, pH, and contamination. One liter of a sterile 2% glycerol solution containing 0.1 g/L streptomycin, 0.04 g/L chloramphenicol, 6 mL/L ethanol, and 100 mL of Antifoam A was added to the fermentor as necessary to maintain culture volume. Usually, 2−3 additions were needed over the 5-day fermentation.

On the fifth day, cells were harvested and C102T was purified by a modification (*21*) of the standard protocol (*23*). Protein was oxidized with $K_2Fe(CN)_6$, which was then removed by use of a small Sephadex DEAE A25 column prior to the second ion-exchange column. Following the final ion-exchange column and dialysis into NMR buffer, protein was concentrated by use of centrifugal filters (Centricon). A few grains of sodium dithionite were added to the concentrated sample to reduce the protein. For experiments involving reduced protein, the acetate NMR buffer contained 12 mM ascorbate and a grain of sodium dithionite to maintain a reducing environment in solution. Protein composition was confirmed by electrospray mass spectroscopy.

Nuclear Magnetic Resonance Spectroscopy. NMR data were acquired at 25 °C on a Bruker Avance DRX 500 spectrometer. [*U*-^{15}N]C102T protein samples were dissolved in 50 mM deuterated acetate, pH 4.6 (uncorrected). Dioxane was added as the internal standard. Spectra were processed on a Silicon Graphics workstation with FELIX 970 (Molecular Simulations, Inc.).

[^{1}H−^{15}N]NOESY−HSQC spectra were collected on oxidized (0.2 mM) and reduced (0.3 mM) C102T protein samples. WATERGATE (*24*) pulses were incorporated into pulse programs for water suppression. States-TPPI phase cycling was used in both indirect dimensions. The initial t_2 sampling delays were adjusted to half the value of the t_2 increment to eliminate phase errors and baseline distortion. Frequency jumping was used to center the proton spectrum in the amide region. A mixing time of 133 ms and recycle time of 1.5 s was used. For the oxidized protein, a total of 512 complex points were collected in t_3, with a spectral width of 2155 Hz, centered at 8.15 ppm; 128 complex points were

collected in T_1, with a spectral width of 6500 Hz, centered at the water frequency; 32 complex points were collected in t_2, using a spectral width of 1250 Hz and the ^{15}N carrier at 118.5 ppm. For each t_1 increment, 16 scans were acquired. For the reduced protein, a total of 1024 complex points were collected in t_3, with a spectral width of 2790 Hz, centered at 8.00 ppm; 128 complex points were collected in t_1, with a spectral width of 6500 Hz, centered at the water frequency; 32 complex points were collected in t_2, using a spectral width of 1250 Hz and the ^{15}N carrier at 118.5 ppm. For each t_1 increment, 16 scans were acquired. For both spectra, an exponential line-broadening function was applied in ω_3; shifted sine bell functions were used to apodize the data in the indirect dimensions. The data were zero-filled once in each indirect dimension before Fourier transformation.

A series of [^{1}H−^{15}N] correlation spectra were collected to determine the backbone ^{15}N longitudinal (R_1) and transverse (R_2) relaxation rate constants. Pulse sequences used to measure relaxation rates have been described previously (*25*) as well as the PEP-Z modification (*26*). The initial t_1 sampling delays were adjusted to half the value of the t_1 increment. Recyle times of 1.5 s were used for all experiments. For R_1 experiments, relaxation delays of 17.3 (×2), 207, 345, 518, 777, and 2500 (×2) ms were used (duplicate acquisitions noted by ×2). For R_2 experiments, relaxation delays of 8.14 (x2), 16.29, 24.43 (×2), 32.58 (×2), 40.72, 57.01, 73.30, 146.59 (×2), 171.02, 219.88, and 472.35 (×2) ms were used. No data were collected at 472.35 ms for the reduced protein in order to reduce the data collection time and minimize the chance that the protein would become oxidized. The interval between the refocusing pulses in the ^{15}N CPMG sequence was 1 ms. For oxidized C102T spectra, a total of 2048 complex points were collected in t_2, with a spectral width of 2155 Hz, centered at 8.15 ppm; 128 complex points were collected in t_1, using a spectral width of 1800 Hz and the ^{15}N carrier at 118.5 ppm. For each t_1 increment, 32 scans were acquired. For reduced C102T spectra, a total of 2048 complex points were collected in t_2, with a spectral width of 2155 Hz, centered at 8.00 ppm; 128 complex points were collected in t_1, using a spectral width of 1250 Hz and the ^{15}N carrier at 118.5 ppm. For each t_1 increment, 32 scans were acquired. For all spectra, a 3 Hz exponential line broadening function was applied in ω_2; shifted sine bell functions were used to apodize the data in ω_1. The data were zero-filled once in ω_1 before Fourier transformation.

Relaxation Data Analysis. Individual peak heights were measured by use of FELIX macros written by Dr. M. Akke (Lund University) and supplied by Dr. A. G. Palmer (Columbia University). Uncertainties in peak heights were estimated from duplicate spectra as described previously (*25*). R_1 and R_2 measurements were determined by nonlinear, least-squares fitting of the experimental peak heights versus time using monoexponential functions provided in software packages by Dr. A. Palmer (Columbia University) or in KaleidaGraph (Synergy Software). KaleidaGraph was used to visualize the fits to the data.

The model-free formalism was used to relate the relaxation parameters to the spectral density function of the NH bond vector. The relaxation rates, R_1 and R_2, for an amide ^{15}N nucleus are dominated by dipolar interaction with the directly attached proton and by chemical shift anisotropy (*27*):

$$R_1 = (d^2/4)[J(\omega_H - \omega_N) + 3J(\omega_N) + 6J(\omega_H + \omega_N)] + c^2J(\omega_N) \quad (1)$$

$$R_2 = (d^2/8)[4J(0) + J(\omega_H - \omega_N) + 3J(\omega_N) + 6J(\omega_H) + 6J(\omega_H + \omega_N)] + (c^2/6)[4J(0) + 3J(\omega_N)] + R_{ex} \quad (2)$$

for which the constants $d = [\mu_0 h\gamma_N\gamma_H/8\pi^2]\langle r_{NH}^3\rangle$ and $c = \omega_N\Delta\sigma/\sqrt{3}$; μ_0 is the permeability of free space; h is Planck's constant; γ_N and γ_H are the gyromagnetic ratios of the proton and nitrogen nuclei, respectively; ω_H and ω_N are the ^{1}H and ^{15}N Larmor frequencies, respectively; r_{NH} is the internuclear ^{1}H−^{15}N distance (1.02 Å); and $\Delta\sigma = -160$ ppm is the chemical shift anisotropy measured for ^{15}N nuclei (*28*). Exchange contributions to R_2, due to conformational averaging on the microsecond−millisecond time scale, are treated by the third term, R_{ex}, in eq 2.

In addition, contributions from paramagnetic effects lead to additional terms in these equations (*29*, *30*). For low-spin ($S = ^1/_2$) systems, these terms are negligible for protons that do not experience contact shifts and are >7 Å distant from the heme iron (*31*). In addition, due to the dependence of paramagnetic relaxation on the square of the nuclear magnetogyric ratio (γ^2), the effect is further reduced (about 100-fold) for nitrogen nuclei (*63*). For oxidized C102T, amide nitrogens outside an 8 Å radius from the heme iron are negligibly perturbed by the paramagnetic metal and were treated as diamagnetic in these studies. Analysis of ^{15}N relaxation behavior (*32*) of nuclei within the 8 Å radius is beyond the scope of this particular study.

The spectral density functions included in eqs 1 and 2, $J(\omega)$, describe motion in the frequency domain and are the Fourier transforms of the orientational correlation function for the N−H bond vector, describing motions in the time domain. Five spectral density terms, $J(\omega_N)$, $J(\omega_H)$, $J(\omega_N + \omega_H)$, $J(\omega_N - \omega_H)$, and $J(0)$, contribute to the experimental relaxation parameters of eqs 1 and 2. However, the R_1 and R_2 parameters are insufficient to determine the five frequencies that characterize the relaxation parameters as described. Instead, the spectral density function can be represented by a model-free formalism (*33*, *34*) and has been employed for the data presented here. A minimal number of parameters is invoked to describe the overall tumbling rate of a macromolecule and the internal motions of the ^{1}H−^{15}N bond vector:

$$J(\omega) = S^2\,\tau_m/[1 + (\omega\tau_m)^2] + (1 - S^2)\tau/[1 + (\omega\tau)^2] \quad (3)$$

The order parameter (S^2) describes the degree of spatial restriction of the internal motions of the ^{1}H−^{15}N bond vector. The overall correlation time, τ_m, is a result of the tumbling motion of the entire molecule, and τ_e is the effective correlation time resulting from fast (ps) internal motions, where $1/\tau = 1/\tau_m + 1/\tau_e$. Equation 3 assumes that the overall tumbling of the macromolecule is isotropic. The value of S^2 ranges from 0 to 1, describing motions from completely unrestricted to a relatively fixed molecular frame of reference, respectively.

Analysis of the relaxation data within the model-free formalism was performed with the Modelfree program, version 3.1, kindly provided by Dr. A. G. Palmer (Columbia University) and described in previously published procedures

(*35*). The relaxation data for each resonance were fit to three different dynamical models while τ_m was held fixed: (1) S^2, (2) S^2 and τ_e (3) S^2 and R_{ex}. Initial estimations of the overall correlation times, τ_m, were obtained from the 10% trimmed mean of R_1/R_2. A grid search was used to obtain initial guesses for other model parameters. Model selection was carried out as described by Mandel et al. (*35*), with some adjustments since only R_1 and R_2 were used in the calculations. The statistical approach was not applicable for model selection since the fits for models 2 and 3 had zero degrees of freedom. Instead, models 2 and 3 were used only when the sum squared error (SSE) >15 for model 1 fits, errors in predicted τ_e and R_{ex} values were less than predicted values, and R_{ex} terms were greater than 1 s.

RESULTS

Optimization of Fermentation and Purification of ^{15}N-Labeled Iso-1-cytochrome c. The first step in performing heteronuclear NMR experiments on any protein is to produce large quantities of labeled protein. This is typically done by inserting the gene encoding the protein of interest into an expression plasmid and expressing large amounts of protein in a well-developed expression system (*36*, *37*). Unfortunately, mitochondrial cytochromes *c*, including yeast iso-1-cytochrome *c*, are not easily expressed in prokaryotic expression systems. *C*-type cytochromes are characterized by a prosthetic heme group that is linked to the protein via thioether bonds to two cysteine side chains. During biosynthesis of the holoprotein, the covalent attachment is catalyzed by a mitochondrial protein called heme lyase (*38*, *39*), a protein that is not present in prokaryotic expression systems. When this enzyme is not present, heme is not attached and holoprotein is not formed.

To correctly express isotopically labeled iso-1-cytochrome *c*, we aimed to develop an economical method for production directly in yeast. Isotopic labeling requires growth in a defined, minimal medium so that sources of carbon, nitrogen, and other nutritional sources can be strictly controlled. In the standard protocol for production of cytochrome *c*, a haploid yeast strain is grown in rich (YPD) medium for 4−5 days, cells are autolysed in ethyl acetate, and cytochrome *c* is purified by ion-exchange chromatography (*21*, *23*). Typical yields for wild-type iso-1-cytochrome *c* are 25−35 mg/5 L of medium. Growth according to the same protocol except in minimal synthetic dextrose (SD) medium decreased this yield to less than 0.5/L, an amount that is insufficient for economical production of labeled protein.

To optimize a protocol for improving the yield of cytochrome *c*, cultures of C93d were grown in 10 mL batches under a variety of media conditions. The culture density was recorded at various times during growth. After 15 h of growth, the cells were subjected to low-temperature spectroscopy to determine the amount of holocytochrome *c* that was produced by the cells. In these small test cultures, we tested the effect of the addition of Celtone, various Celtone/ammonium sulfate ratios, addition of buffers and the effect of buffer concentration, the addition of various salts, and the addition of glycerol. We aimed to produce a protocol that optimized both culture growth and the production of holocytochrome *c*.

Addition of buffer to the SD medium was found to be necessary, as the pH of the medium can drop over long fermentation times. Bis-tris was found to be appropriate for this purpose, but concentrations over 50 mM inhibited culture growth (data not shown). SD medium with added 40 mM Bis-Tris buffer produced cultures with high cell counts, but they made very little cytochrome *c* (compare thin dotted lines in Figure 1 panels A and B). Addition of Celtone to the medium increases the culture density somewhat but increased the production of holocytochrome *c* slightly (compare thick dashed lines in Figures 1 panels A and B). We found that spiking the fermentor flask with glycerol and/or ethanol toward the end of the fermentation period increased the production of holocytochrome *c* significantly (Figure 1). These experiments also showed that the Celtone required filter sterilization, that concentrations of ammonium sulfate greater than 2 mg/mL inhibited growth, and that addition of some salts to the medium increased cell growth and cytochrome *c* production (data not shown). C93d grown in minimal medium composed of 1.3 mg/mL Celtone and 2 mg/mL ammonium sulfate, buffered with 40 mM Bis-Tris, and spiked with glycerol or ethanol toward the end of the culture grew to a density of 70(±3)% and produced 90(±2)% of the amount of holocytochrome *c* found in a culture of C93d grown in 10 mL YPD cultures. These culture conditions, which yielded the most in vivo cytochrome *c* as determined by low-temperature spectroscopy, were scaled up to a 5-L fermentor batch. Using the protocol described in Materials and Methods, we produced 2 mg of ^{15}N-labeled

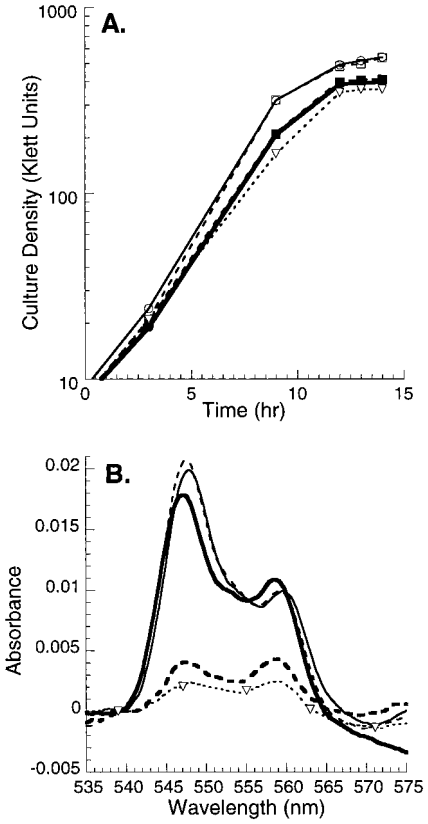

FIGURE 1: Growth curves (A) and low-temperature spectroscopy (B) of test cultures of diploid C93, the yeast strain expressing C102T, comparing the cell growth with the expression of iso-1-cytochrome *c*. In both panels the thin dashed line is YPD alone; the thin solid line is YPD with a glycerol spike toward the end of the growth period; the thick dashed line is SD (synthetic dextrose) with Celtone-U and 40 mM Bis-Tris; the thick solid line is SD with Celtone-U and 40 mM Bis-Tris, spiked with glycerol; the thin, dotted line (▽) is SD with 40 mM Bis-Tris only.

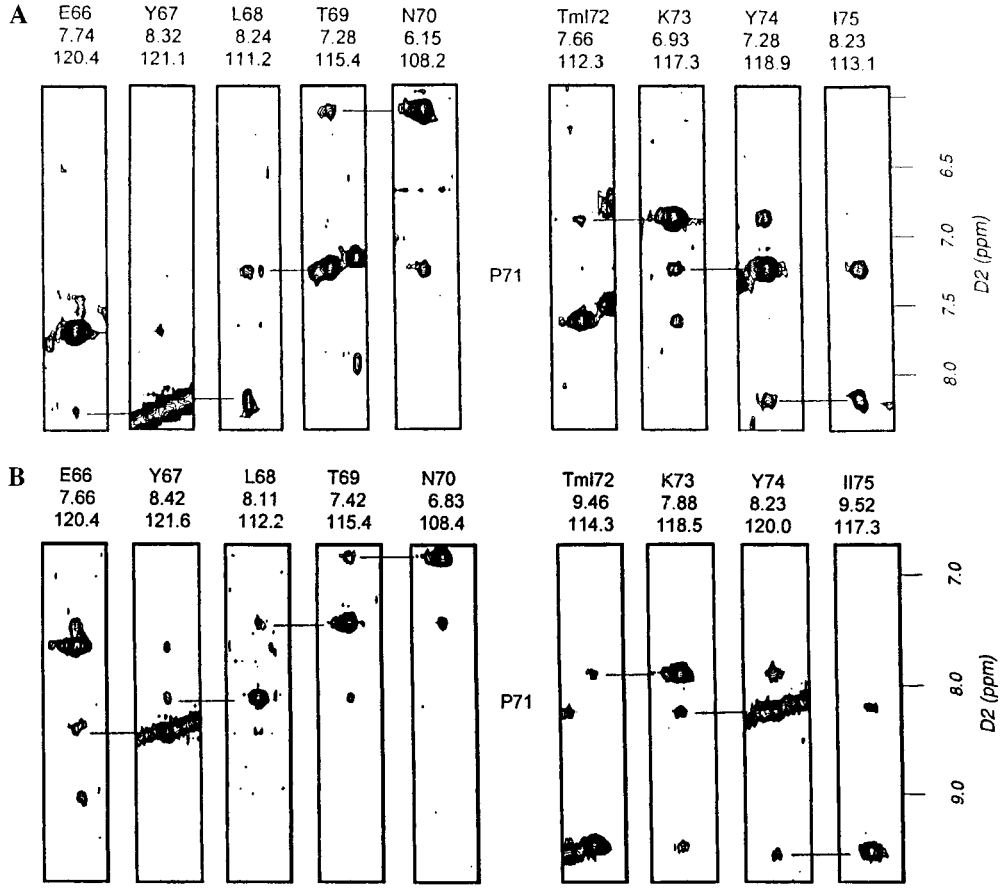

FIGURE 2: Sequential ^{15}N backbone amide resonance assignments are based on [$^{1}H-^{15}N$] NOESY−HSQC experiments. Representative slices from the 3D [$^{1}H-^{15}N$] NOESY−HSQC datasets (collected and processed as described in Materials and Methods) demonstrating connectivities through the 60s helix and into loop D in both reduced (A) and oxidized (B) [*U*-^{15}N]C102T. Sequential amide−amide (d_{NN}) connectivities are highlighted with horizontal lines between strip plots. Even in irregular, nonhelical segments of the protein, sequential connectivities were found for the majority of resonances in the protein.

C102T in 5 L of medium, enough to produce a 500 μL, 0.3 mM protein sample. Although the cytochrome *c* yield did not scale up from the 10 mL test cultures as we had anticipated, the amount of protein produced by one 5-L fermentor run was sufficient for heteronuclear, multidimensional NMR experiments.

Mass spectroscopic analysis showed that C102T grown on unlabeled minimal medium using our protocol was indistinguishable from the protein grown on rich medium. [*U*-^{15}N]C102T produced by this protocol was analyzed by electrospray mass spectroscopy and determined to be correctly expressed (MW = 12 859). The expected mass reflects >99% ^{15}N incorporation, the presence of the trimethylated lysine (Tml) 72, and covalently attached heme.

^{15}N Resonance Assignments for Reduced and Oxidized C102T. Iso-1-cytochrome *c* contains five extra residues at the amino terminus when aligned with other eukaryotic cytochromes *c*; thus, we followed the convention of numbering its residues from −5 to 103. C102T is composed of 108 residues, four of which are prolines and nine of which are asparagine or glutamine. Gao et al. (*15*) published proton assignments for oxidized and reduced C102T at 300 K, pH 7.0. Recently, additional proton assigments for oxidized and reduced C102S iso-1-cytochrome *c* at 303 K, pH 7.0, have been published (*6*, *7*). About 40% of the amide resonances in the NMR spectra collected for [*U*-^{15}N]C102T can be assigned on the basis of their unique proton chemical shifts and direct comparison to previously published amide proton chemical shifts. Although the NMR data reported here were collected under slightly different temperature and pH conditions, proton amide resonance assignments were in agreement with previously published assignments within the spectral resolution of the experiments.

To confirm and extend the ^{15}N backbone assignments, 3D [$^{1}H-^{15}N$] NOESY−HSQC data sets were collected. Representative slices from the 3D [$^{1}H-^{15}N$]NOESY−HSQC data sets are shown in Figure 2. Connectivities through the 60s helix and into loop D are shown to demonstrate the quality of the sequential data even in less regular regions for relatively dilute (<0.5 mM) oxidized and reduced C102T NMR samples. Independent data from these spectra, including sequential amide−amide (d_{NN}) connectivities and sequential α-amide ($d_{\alpha N}$) connectivities, were used to sequentially assign the amide nitrogen resonances. The ^{15}N resonance assignments for both oxidized and reduced iso-1-cytochrome *c* (C102T) are provided in Table S1 (Supporting Information).

The 3D [$^{1}H-^{15}N$] NOESY−HSQC experiment allowed us to unambiguously assign ^{15}N chemical shifts for 91 residues in the reduced form of the protein and for 90 residues in the oxidized form. The two N-terminal residues, Thr −5 and Glu −4, are still unassigned sequentially. Due to overlapping resonances, broadened resonances that result in a reduced signal-to-noise ratio, a lack of sequential NOE connectivities, and other ambiguities, other ^{15}N resonances remain unassigned. For the reduced protein, Phe −3, Asn

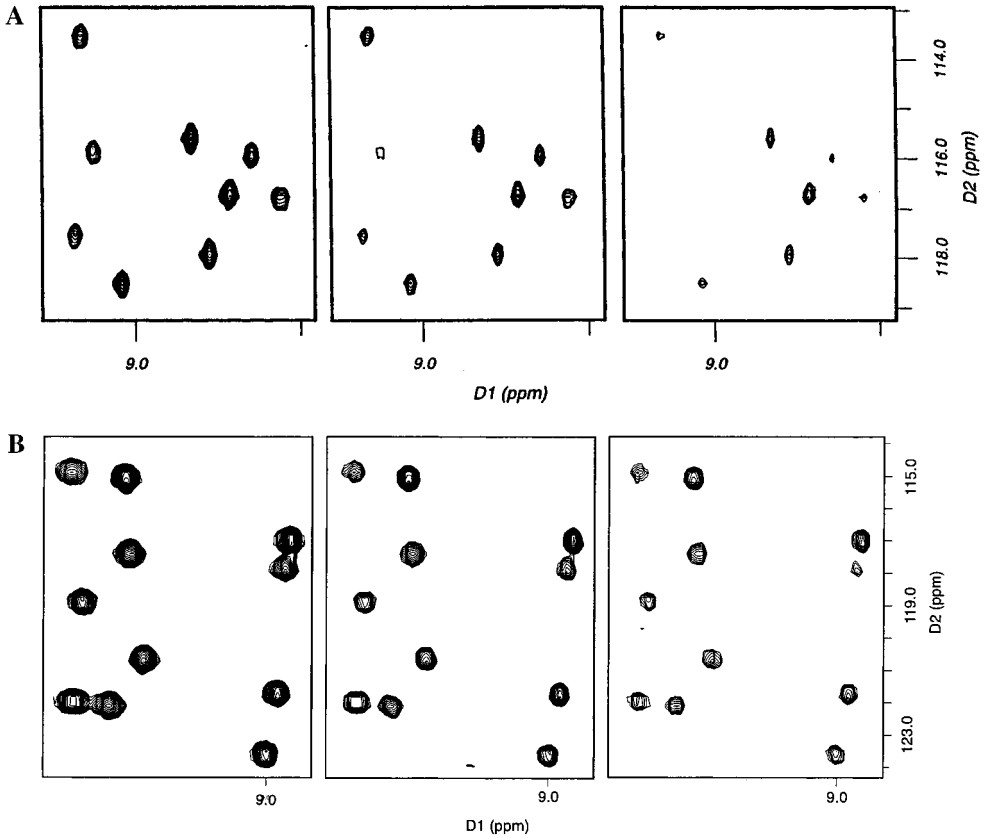

FIGURE 3: Expanded regions from T_1 spectra of both reduced (A) and oxidized (B) [$U-^{15}$N]C102T are shown to demonstrate not only the quality of the spectra but also the similarity of the resonance line widths and decay times for the diamagnetic and paramagnetic forms of the protein. Panels from left to right represent T_1 experiments collected with relaxation delays of 17.3, 207, and 345 ms, respectively. Experimental parameters and spectral processing are described in Materials and Methods.

31, Leu 32, His 33, His 39, Gly 41, Glu 61, Thr 78, Gly 83, Gly 84, and Leu 85 are unassigned sequentially. For the oxidized protein, His 18, Gly 29, Asn 31, His 33, His 39, Asp 60, Lys 79, Met 80, Lys 81, Gly 83, Gly 84, Leu 85, and Lys 87 remain unassigned. These amide resonances are largely contained in loops where there is a lack of sequential information to unambiguously assign the residues on the basis of NOE data only. Others overlap with other resonances, making a conclusive assignment difficult on the basis of NOE data alone. For this study, the imino ^{15}N resonances of the heme group were not assigned.

The ^{15}N paramagnetic shifts for C102T are comparable in relative magnitude and distribution to the proton paramagnetic shifts reported in previous studies (*7, 15*). For the backbone amide group shifts reported here, the paramagnetic shift difference was largely due to the dipolar, or pseudocontact, interactions with the heme iron. The largest ^{15}N paramagnetic shifts (>2.5 ppm) were observed in two regions: a stretch of residues linking the N-terminal helix and loop A (residues Cys 14−Thr 19) and a patch of residues in loop D (Tml 72, Ile 75, and Phe 82). The amides of these residues are within 10 Å of the heme iron, except for Ile 75. For all of these residues, the proton paramagnetic shifts are greater than 1 ppm, in agreement with NMR data reported previously (*15, 7*). Another stretch of residues (Lys 27 through Leu 32) is within 10 Å of the heme. Complete, unambiguous assignments were not obtained for this entire stretch, although Lys 27 had a ^{15}N paramagnetic shift of only 0.15 ppm.

^{15}N Relaxation Rate Measurements. With most of the ^{15}N backbone resonance assignments in hand, a series of heteronuclear 2D experiments were collected to measure ^{15}N relaxation rates, R_1 and R_2, of backbone amide nitrogen atoms in the oxidized and reduced forms of C102T. Figure 3 shows expanded regions from the T_1 spectra of both oxidized and reduced C102T to demonstrate not only the quality of the spectra but also the similarity of the resonance line widths for the diamagnetic and paramagnetic forms of the protein. For the oxidized protein, relaxation times for 70 amide nitrogens are reported; for the reduced protein, relaxation times for 69 are reported here. Missing data for assigned resonances are due primarily to resonance overlap, which caused difficulty in measuring peak height intensities. Additionally, reliable decay curves could not be measured for resonances that were broadened and weak in the [^{15}N−^{1}H] HSQC spectra due to fast solvent exchange or paramagnetic effects (for residues near the heme iron in the oxidized form).

Representative T_1 and T_2 relaxation decay curves, peak intensity plotted against time, are shown in Figure 4. Single-exponential two- and three-parameter decay curves were fit to the peak intensity decay data. In particular, intensity data for amide nitrogens close to the heme iron in the oxidized form were also adequately fit by two-parameter decay curves, demonstrating the lack of effect of the paramagnetic iron on the relaxation rates. Relaxation data are reported for amides throughout the paramagnetic (oxidized) form of the protein. (Analysis of backbone dynamics is presented only

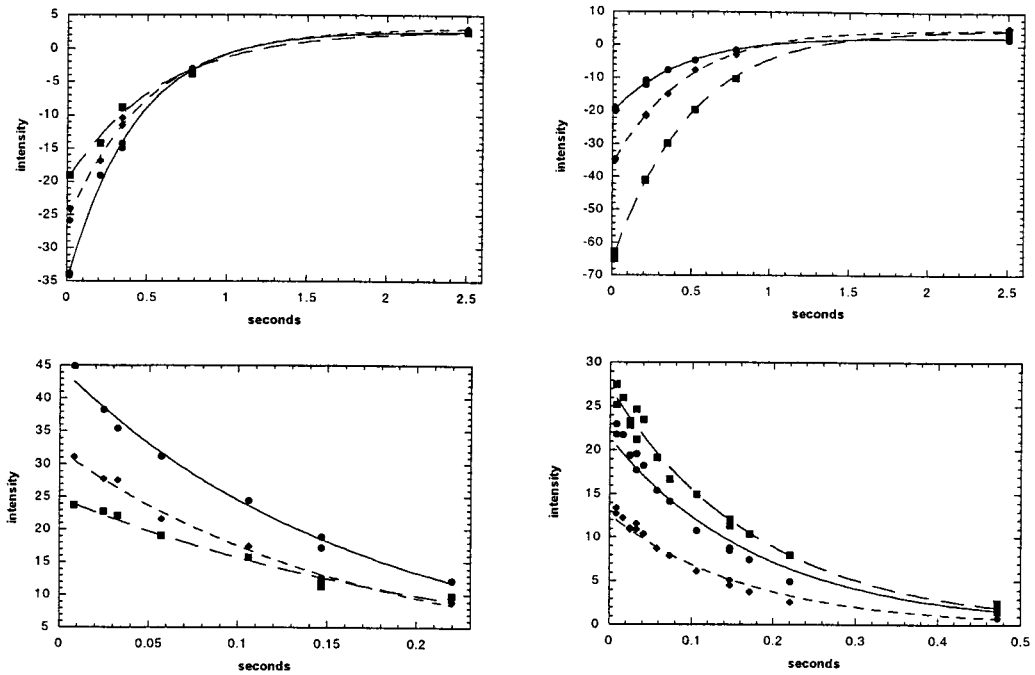

FIGURE 4: Examples of T_1 and T_2 relaxation decay curves for selected residues contained in various structural elements of reduced (left panels) and oxidized (right panels) of [*U*-^{15}N]C102T. Resonance peak intensity is plotted against time (seconds) and curves indicate fits to inversion−recovery data (T_1, top two panels) and single-exponential decays (T_2, bottom two panels). Error bars would be smaller than the size of characters used to indicate data points. Top left: T_1 data for Cys 14 (■), Gly 45 (◆) and Lys 99 (●). Bottom left: T_2 data for Lys 27 (■), Glu 66 (◆) and Ala 101 (●). Top right: T_1 data for Ser 40 (◆), Asn 62 (■) and Ile 75 (●). Bottom right: T_2 data for Ala −1 (■), Leu 68 (◆) and Ala 101 (■).

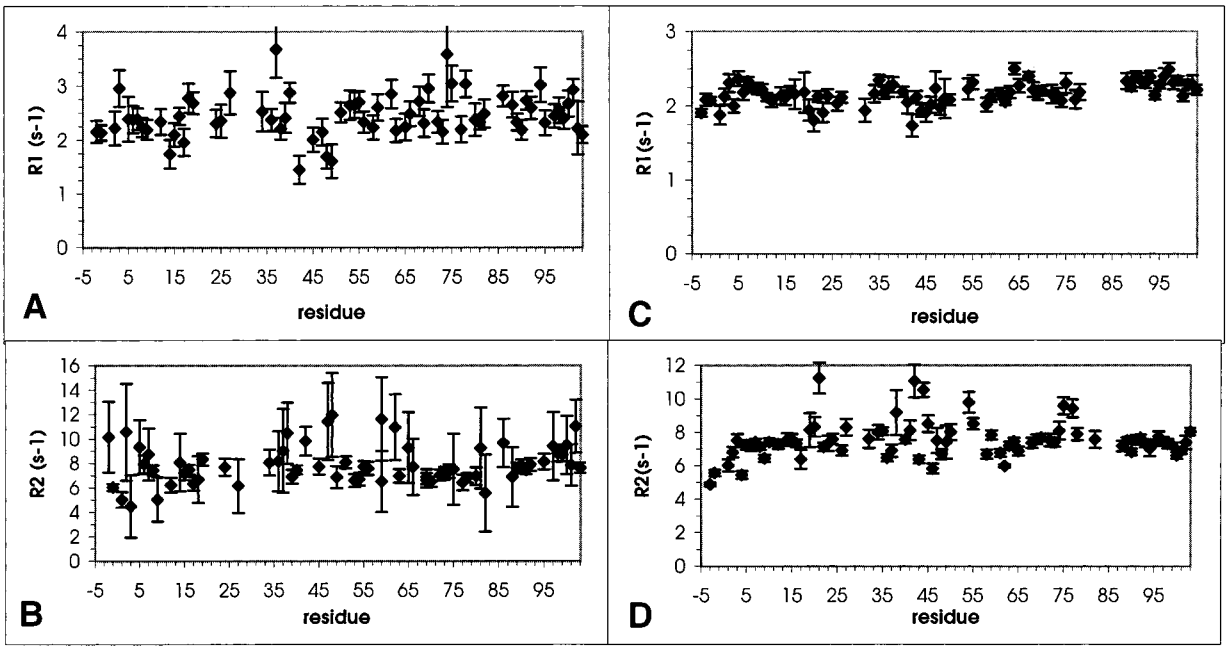

FIGURE 5: Experimental values for relaxation rates, R_1 and R_2 (in seconds^{-1}), are shown for both the oxidized and reduced forms of C102T, plotted against residue number. Measured R_1 rates are shown in panels A (reduced [*U*-^{15}N]C102T) and C (oxidized [*U*-^{15}N]C102T). Measured R_2 rates are shown in panels B (reduced [*U*-^{15}N]C102T) and D (oxidized [*U*-^{15}N]C102T). Gaps in the data result from overlapping resonances, broadened resonances, and unassigned amide resonances that made measurements unavailable. Error bars for measured rates are shown.

for those residues greater than 8 Å from the heme iron, see below.)

The experimental values for relaxation rates, R_1 and R_2, plotted against residue number are shown in Figure 5 for both oxidized and reduced forms of C102T. The average value of T_1 (= $1/R_1$) for the reduced protein was 418.9 ± 44.5 ms; in the oxidized protein, the average T_1 was 470.3 ± 23.1 ms. The average value of T_2 (= $1/R_2$) for the reduced protein was 130.7 ± 23.3 ms; in the oxidized protein, the average T_2 was 140.6 ± 6.9 ms. The errors in the relaxation rates calculated for the reduced protein were somewhat larger than for oxidized protein, since fewer time points and duplicate data sets were collected for the reduced protein.

Regions of C102T having amide nitrogens with R_1 relaxation rates significantly different from the mean are few (Figure 5). A region in the reduced form of C102T, from

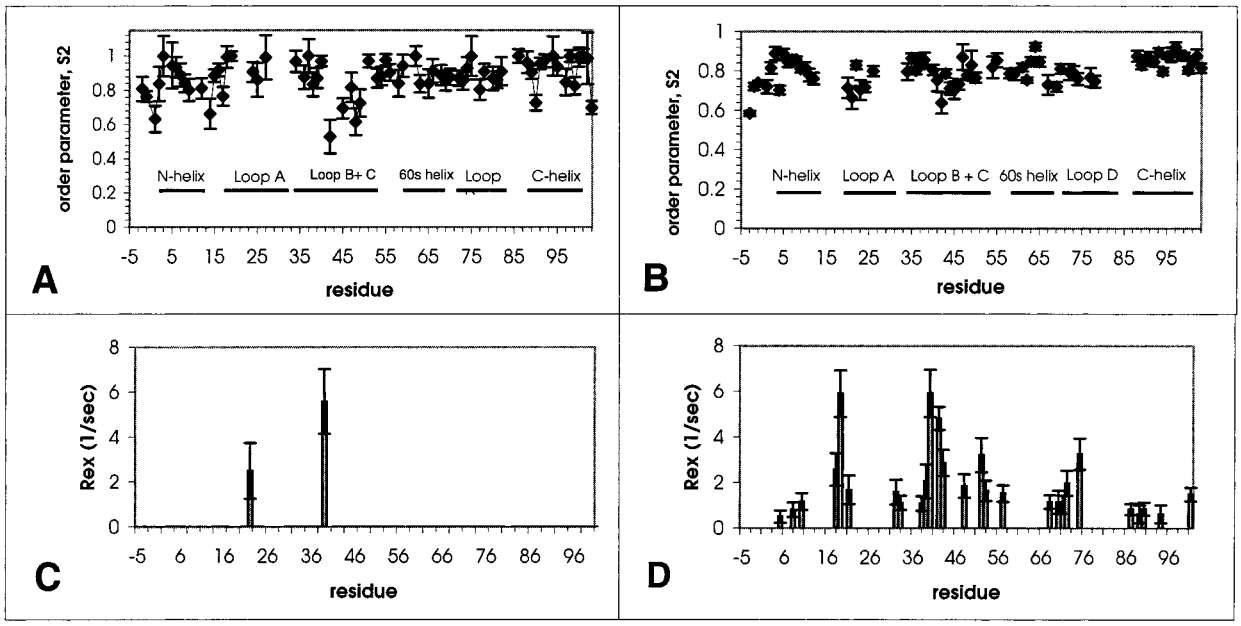

FIGURE 6: Order parameters (S^2) for backbone nitrogens measured for backbone nitrogen nuclei in reduced (A) and oxidized (B) [*U*-^{15}N]-C102T are plotted as a function of residue number. Characteristic structure elements of C102T are represented by labeled bars in plot. Residues for which spectral density function fits required an additional exchange term are shown in panels C (reduced C102T) and D (oxidized C102T). Predicted exchange rates (R_{ex}, seconds^{-1}) are plotted against residue number.

Gln 43 to Tyr 48, shows a discernible reduction in R_1 relaxation rates relative to the average. These residues are part of the overlapping loop B/C region of the protein. The same region in the oxidized form of the protein does not show significantly lower than average R_1 relaxation rates.

The R_2 relaxation rates along the backbone of the reduced form of C102T are uniform within experimental errors. In the oxidized form of the protein, however, more variation is seen, particularly in the loop regions. Loop residues that show increased R_2 rates are, notably, farther than 8 Å from the paramagnetic heme center. Residues with R_2 rates significantly greater than the average include Glu 21 (start of loop A), Gln 42, and Glu 44 (loop B/C overlap region). The amide resonances for Glu 21 and Gln 42 have greater than average line widths, further indicating that these loop residues may be involved in slow (microsecond−millisecond) conformational exchange processes.

Model-Free Analysis. The principal components of the inertia tensor for C102T were derived from the crystallographic structures (1YCC and 2YCC) (*2*, *9*). The relative values are 1:1.28:1.47; thus, isotropic tumbling of the protein as a globular sphere was assumed for further analysis of the ^{15}N relaxation rate data. Based on the paramagnetic shift data and relaxation rate data, we noted that the heme iron affected only amides within an 8 Å radius. These observations are consistent with calculations of the paramagnetic contribution to relaxation, which predict protons and, thus, nitrogens outside a 7 Å radius would be minimally affected (*31*) by the Fe(III) state of the iron ($S = {}^1/_2$). Consequently, a more detailed analysis of backbone dynamics was not carried forward for five assigned amides (Cys 14, Cys 17, Met 80, Ala 81, and Phe 82) within a conservative 8 Å cutoff and remaining nuclei were treated as diamagnetic.

Initial estimates of the overall correlation time (τ_m) were based on the 10% trimmed mean of the R_2/R_1 ratios. In addition, for calculations involving oxidized C102T, as indicated earlier, the five amides within an 8 Å radius of the heme iron were discarded from this set of data. The resulting initial estimate for both oxidation states was 5.6 ± 0.04 ns. By use of the calculated overall correlation times, the experimentally determined relaxation rates, R_1 and R_2, were fit to spectral density functions to calculate order parameters (S^2).

The experimental data were fit to spectral density functions containing only one or two adjustable parameters. The effective correlation time, τ_e, and a conformational exchange parameter, R_{ex}, were included as extra terms for residues not adequately fit by the simple spectral density function (S^2 only, or model 1). A rigorous statistical approach for model selection (*35*) was not possible since only two experimental parameters, R_1 and R_2, were available, as described in Materials and Methods. Only two out of the 69 residues fit in the reduced form required an extra term to fit the experimental relaxation data (Figure 6C). In contrast, 27 out of the 70 residues (Figure 6D) fit in the oxidized form required the additional R_{ex} exchange term (model 3). Relaxation data for all residues studied, in both forms, were adequately fit by these criteria. Once spectral density models were selected, the overall correlation time (τ_m) was optimized for all residues simultaneously. The optimized correlation time for the reduced protein was 5.18 ± 0.07 ns; the optimized correlation time for the oxidized protein was 5.26 ± 0.03 ns. Thus, the overall tumbling times for both forms of the protein were the same within 1 standard deviation of each other. In addition, these calculations underscore the fact that the contribution from the low-spin ($S = {}^1/_2$) paramagnetic metal has a negligible effect on the relaxation behavior of the vast majority of the backbone ^{15}N nuclei in the oxidized form of C102T.

Backbone Dynamics of Reduced C102T. The average order parameter values for the different helices and loop structures in C102T are listed in Table 1. For the reduced form of the protein, only loop C had a reduced average order parameter (0.79 ± 0.06) relative to the rest of the structure; however,

Table 1: Average Order Parameter Values (S^2) for Structural Elements[a]

structural element	residues	reduced C102T	oxidized C102T
N-helix	3−13	[7/11] 0.89 (0.07)	[10/11] 0.82 (0.06)
loop A	17−32	[6/16] 0.92 (0.09)	[6/16] 0.73 (0.06)
loop B	34−45	[8/12] 0.84 (0.16)	[11/12] 0.78 (0.07)
loop C	40−54	[9/15] 0.79 (0.15)	[11/15] 0.77 (0.06)
60s helix	60−70	[7/10] 0.89 (0.06)	[8/11] 0.81 (0.07)
loop D	71−84	[9/14] 0.89 (0.06)	[5/14] 0.77 (0.02)
C-helix	87−103	[14/17] 0.92 (0.10)	[16/17] 0.86 (0.03)

[a] Number of residues measured out of total residues in each element is noted in brackets. Standard deviations are given in parentheses.

the average is not outside the error range of average S^2 values for other structural elements. Specifically, Gln 42, Gly 45, Tyr 48, and Thr 49 contributed the most to lowering the average for this region of the protein. The only two residues in the reduced form requiring an R_{ex} term were Gly 24 and Gln 42. Both residues are contained in loop structures, although not all loops in the protein have lower than average order parameters.

Backbone Dynamics of Oxidized C102T. In the oxidized form of the protein, a slight difference in average S^2 values between helices and loops can be observed. As listed in Table 1, the C-helix in the oxidized form has the highest average order parameter value (0.86 ± 0.03). The loop structures all have average S^2 values lower than 0.8, although the difference is not necessarily significant since several residues in loops A and D were not included in the analysis due to their proximity to the paramagnetic heme iron or lack of sequential assignments. As seen for the reduced form, below-average order parameters are observed for a stretch of loop C residues (Gln 42, Glu 44, Gly 45, and Tyr 46). In addition, residues at the amino-terminus (Phe −3 and Lys −2) and contained in loop A (Gly 23 and Gly 24) also have lower than average order parameters.

Strikingly, in oxidized C102T, the pattern of residues requiring R_{ex} terms was much more widespread than observed in the reduced form. Twenty-five residues of the oxidized form of the protein required R_{ex} terms. Notably, no residues in the 60s helix (Asp 60−Thr 69) required an additional exchange term; however, the pattern of residues requiring R_{ex} terms was not strongly correlated with structural elements. The average value of the R_{ex} term was 1.79 s^{-1}, but the residues requiring the largest R_{ex} values were Glu 44 (4.81 ± 0.51 s^{-1}) and Gln 42 (5.92 ± 1.1 s^{-1}). The requirement for R_{ex} terms in fitting the relaxation data to a spectral density model implies that there is significant motion within the protein on time scales at least an order of magnitude slower than the overall correlation time (5.2 ns).

Comparison of Order Parameters for Oxidized and Reduced C102T. The order parameter, S^2, largely reflects the nanosecond−picosecond time scale motions along the backbone. The average order parameter (S^2) calculated for all amides in the backbone of the reduced form of C102T was 0.88 ± 0.10.The average for the oxidized form was 0.80 $\pm$ 0.07; thus, the overall averages are slightly, but not significantly, different. To determine if this difference in average order parameter could be attributed to a particular segment of the protein in one redox form compared to the other or if it reflected the larger errors from the relaxation data for the reduced protein, a more detailed analysis was undertaken.

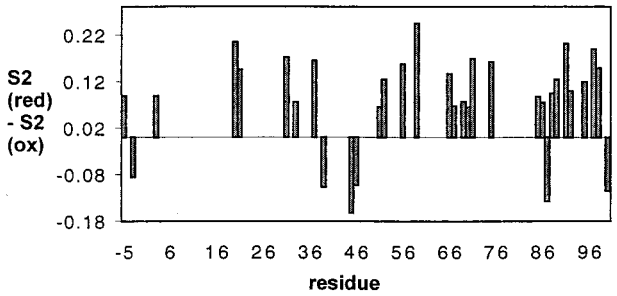

FIGURE 7: Order parameter changes linked with redox state are shown. Difference between order parameters (S^2) measured for reduced and oxidized [U-^{15}N]C102T ($S^2_{red} - S^2_{ox}$) is plotted against residue number. Only significant changes in order parameters are plotted. Positive differences indicate a gain in order on the picosecond to nanosecond time scale linked to reduction; negative differences indicate loss in order linked to reduction.

The difference in order parameters between oxidized and reduced C102T are plotted versus residue number in Figure 7. Thirty-two residues were found to have significant S^2 differences between the oxidized and reduced forms. The majority (26) of these residues had higher order parameters in the reduced form compared to the oxidized form. These 26 residues were distributed throughout the protein. Only two structural elements had continuous clusters of significant changes. First, the C-terminal helix contains a stretch of residues having significant order parameter differences between the redox forms of the protein. Second, the N-terminal segment of loop D (Tml 72−Thr 78) had significant increases in order parameter values in reduced C102T compared to oxidized. Neither stretch of residues is near (<8 Å) the paramagnetic iron in space.

Additionally, a number of residues in overlapping loops B and C have significant changes in order parameters upon reduction. Interestingly, significant increases in order parameter values were seen for three loop B residues (Gly 34, Phe 36, and Gly 37), while significant decreases upon reduction were observed for three residues in loop C (Gln 42, Tyr 48, and Thr 49). Only three other residues (Gly 1, Asp 90, and Glu 103) had significant decreases in order parameter values upon reduction.

DISCUSSION

Isotopically Labeled Cytochrome c for NMR Studies. We have described a method for expressing and purifying [U-^{15}N]iso-1-cytochrome *c*. By taking advantage of constitutively expressed heme lyase activity, we can produce correctly expressed, postranslationally modified, and folded C102T for structural studies. By use of commercially available media supplements, only minor modifications to established media recipes and fermentation protocols were necessary to provide a suitable medium for robust fermentation and uniform isotopic incorporation. Mass spectroscopic and NMR techniques demonstrated that ^{15}N was uniformly incorporated into the protein. [U-^{15}N]C102T was isolated with straightforward methods published previously (*19*). While the yield of ^{15}N-labeled protein was not high (on average, 0.5 mg/L), sufficient amounts were available at a reasonable cost for the NMR-based structural studies. Furthermore, since C102T is a very stable protein, one

preparation provided enough well-behaved protein for multiple studies over several months, a favorable point in cost considerations. The availability of isotopically labeled iso-1-cytochrome *c* opens new avenues to using NMR techniques for testing structure−function relationships and the protein−protein interactions that guide the electron transport function of this small, but important, heme protein.

Recently, *Escherichia coli* expression systems have been developed to produce iso-1-cytochrome *c* (*40*). Respectable yields (15 mg/L) of unlabeled, heme-containing protein expressed in rich medium were reported, but the lysine residue at position 72 was not trimethylated. The yields in minimal, isotopically labeled medium have not yet been reported. Nonetheless, the flexibility and malleability of the *E. coli* expression systems promise that these problems can be overcome. While isotopic labeling in the *S. cerevisiae* expression system might turn out to be more costly, the advantage is that the protein is correctly posttranslationally modified. Thus, the *S. cerevisiae* expression system promises to be of versatile use for future studies on variant cytochromes *c*, particularly for those studies of the interaction of cytochrome *c* with its redox partners, where correct posttranslational modification could be critical.

^{15}N Chemical Shifts Assigned to Reduced and Oxidized C102T. While detailed structural and dynamic studies of [*U*-^{15}N]-labeled cytochrome b_5 proteins have been presented (*41*), very few prokaryotic, and no eukaryotic, cytochromes *c* have been studied by heteronuclear NMR techniques due to the difficulty in expressing isotopically labeled protein. Heteronuclear backbone assignments for both ferricytochrome *c*′ and ferrocytochrome c_2 from *Rhodobacter capsulatus* and for ferrocytochrome c_{555} from *Chlorobium liminicola* f. *thiosulfatophilum* have been reported previously (*42*, *43*) Since we are now able to produce ^{15}N-labeled cytochrome *c* from *S. cerevisiae*, we report here backbone ^{15}N chemical shift assignments for both reduced and oxidized [*U*-^{15}N]iso-1-cytochrome *c* (C102T). Our methods relied on previously published amide proton assignments and sequential NOE connectivities because of the limiting amount of protein in hand. Our aim was to assign a majority of the backbone amides so that we could carry out two-dimensional heteronuclear experiments to measure hydrogen exchange and relaxation rates. ^{15}N shifts are not reported unless independent NOE data from the current study were available. Sequential amide−amide and α proton−amide connectivities were continuous throughout most of the protein, except for three segments of the amino acid sequence. The two N-terminal residues are still unassigned, as in all NMR studies of iso-1-cytochrome *c* published to date. A lack of NOE connectivities was found for a segment of loop A from Gly 29 to Gly 34 and the linker between loop D and the C-terminal helix from Gly 83 to Leu 85. None of these segments of cytochrome *c* has been implicated in redox-dependent conformational changes or in interactions with redox partner proteins (*4*). Additionally, these regions are not proximal to the heme. Thus, despite some minor gaps in the ^{15}N amide assignments, the coverage along the backbone is significant and useful.

Paramagnetic ^{15}N chemical shift changes along the backbone of C102T largely corresponded with significant amide proton paramagnetic shift differences reported earlier (*5*, *7*). In particular, ^{15}N chemical shift differences greater than 3 ppm were observed for amide nitrogens within roughly a 10 Å radius of the heme iron. Currently, ^{15}N chemical shifts are difficult to calculate and predict (*44*). The ^{15}N chemical shifts are strongly affected by local geometry but are also affected by the strength of the local electrical field. Therefore, the ^{15}N chemical shifts do not necessarily lend quantitative or geometric insight into local conformational differences between redox forms of the protein. Nonetheless, changes in paramagnetic ^{15}N shifts can shed light on conformational changes due to single-site variants in future studies.

Overall Correlation Time Similar for Reduced and Oxidized C102T. The overall correlation times determined for reduced and oxidized C102T do not differ significantly. The average τ_m of 5.2 ns for C102T is in approximate agreement with the 4.0 ns correlation time predicted from electron paramagnetic resonance (EPR) studies of C102T (*45*) and correlation times determined for other proteins of similar size (*46*).

The similarity in correlation times calculated for both redox forms also reflects the negligible effect the paramagnetic iron had on relaxation rates for the majority of amide nitrogens in oxidized C102T. Unpaired spins affect nuclear spin relaxation by contact and dipolar mechanisms and Curie spin relaxation (*47*). The contact mechanism, which is attenuated through bonds between the heme center and affected heme nuclei, does not contribute to the relaxation mechanism for nitrogens of the protein backbone. Dipolar (or pseudocontact) and Curie relaxation mechanisms are linked to overall correlation times. For a protein the size of cytochrome *c*, studied at relatively high magnetic field, pseudocontact and Curie mechanisms of relaxation due to the unpaired spin are expected to have negligible effects on the majority of amide nitrogen relaxation rates (*31*, *48*). Similarly, Banci et al. found that paramagnetic, low-spin Fe(II) had no discernible effect on rotating frame relaxation rates for ^{15}N nuclei within even a 7 Å radius from the heme iron in cytochrome b_5 (*41*).

In this study, amide nitrogens within a conservative 8 Å radius of the heme iron in the corresponding crystal structures (*2*) were excluded from the calculations for determining overall correlation time. The five excluded nitrogen nuclei are located in three segments of the protein: in the linker between the N-terminal helix and loop A, at the C-terminal end of loop A, and in a segment of loop D. Other residues within the 8 Å radius cutoff had amide resonances that were unassigned sequentially.

Backbone Dynamics of Reduced and Oxidized C102T. Relaxation rates were used to predict order parameters for the backbone nitrogens in iso-1-cytochrome *c*. Order parameters (S^2) reflect the fast motions (picosecond−nanosecond) of the ^{15}N−H vector in solution. As predicted from previous structural studies of this globular protein, the order parameter values reported here indicate that both redox forms of the protein are folded and compact. The only stretch of disordered, or highly flexible, amino acids is found at the N-terminus (Thr −5 to Phe −3). Assignments are missing for the two N-terminal residues in both redox states due to a lack of NOEs connecting these residues to the rest of the chain, further suggesting that they are disordered in relation to the rest of the protein.

There is only a weak correlation between order parameters and the different structural elements, helices and loops, in

C102T. In the oxidized form of the protein, the loops had average order parameters less than 0.8; the helices had S^2 averages above 0.8, but the order parameters are within 1 standard deviation of each other. In the reduced protein, the differences were not as marked. ^{15}N relaxation-based studies of SH2 domains (*49*), interleukin 1β (*50*), and staphylococcal nuclease (*51*) also found slightly higher average S^2 values for helices. The backbone dynamics indicate that the loops of C102T are more similar to the loop structures found in the SH2 domain ($\langle S^2 \rangle = 0.76$) than the more flexible linker loops in calbindin ($\langle S^2 \rangle = 0.59$) (*52*), for instance. Crystallographic studies (*4*) and hydrogen exchange studies (*14, 18*) of iso-1-cytochrome *c* confirm that the loops contain hydrogen-bonding networks and many backbone amide hydrogens within the loops are protected from solvent exchange. These loops serve structural purposes, providing heme ligands and linkages and, perhaps, providing epitopes for redox partner recognition. For example, NMR (*53*) and crystallographic (*54*) studies have suggested that the loop D region is at the interfacial surface in the cytochrome *c*−cytochrome *c* peroxidase complex.

Despite the relatively uniform S^2 values determined for both forms of C102T, the residues of loop C (Ser 40−Lys 54) had the most variable relaxation rates and, as a consequence, the average order parameters for this structural element are slightly below the overall S^2 average. In both redox forms, residues in the beginning and middle of the loop sequence (Gln 42, Gly 45, Tyr 48, and Thr 49) had S^2 values significantly lower than the overall average. Interestingly, significant decreases in S^2 upon reduction are observed for three of these loop C residues (Glu 42, Tyr 48, and Thr 49). Additionally, in both redox states, relaxation data for Gln 42 suggest that this particular residue is also subject to slower time scale exchange processes.

Hydrogen exchange experiments (*17*) demonstrate that these residues are not protected from solvent exchange. Similarly, in the crystal structures of both redox forms (*2, 9*), the amides of residues 42, 45, and 48 are not hydrogen-bonded to any other atom. However, in both crystal structures, the amide of Thr 49 is hydrogen-bonded to one of the propionate groups at the bottom of the heme. Crystallographic average thermal factors (*B*-factors) are relatively high for residues in loop C compared to the rest of the structure (*4*). Interestingly, residues at the C-terminal end of the loop (Ser 47−Trp 59), rather than at the N-terminal end, have the highest temperature factors. Loop C does not contain any of the heme ligands or linkages, so it may not play as important a structural role as loops A or D, for instance. Bai et al. (*55*) have suggested that this region in equine cytochrome *c* has a relatively low free energy of unfolding, although it is loop D, not loop C, that is predicted to have the lowest free energy of unfolding in the molecule.

Redox-Dependent Dynamic Behavior. One of the major aims of this study was to examine changes in the dynamic behavior of iso-1-cytochrome *c* that correlate with the oxidation state. Heteronuclear relaxation studies have been used by many other groups interested in dynamic changes in protein backbones correlated with binding events (*49, 52, 56, 57*), folding (*46*), and redox state (*41, 58*). This information, in concert with detailed, high-resolution structural studies, can reveal important changes that impact on our understanding of how proteins function. Using rotating-frame NMR relaxation experiments, Banci et al. (*41*) recently found a difference in backbone dynamics between the two redox states of cytochrome b_5 and identified a general loss of slow motions in the reduced form relative to the oxidized protein. These authors propose that differential flexibility related to redox state may be an important factor underlying molecular recognition processes involving electron-transfer proteins.

We also observed a general increase in order parameters, or a reduction of motions on the picosecond−nanosecond time scale, for the reduced form relative to oxidized C102T. The increased S^2 values for the reduced form were not localized to one region of the protein, rather a loss of fast motions throughout the protein was observed. The increase in order parameters is small relative to changes seen upon gain or loss of secondary structure (*46*), and indeed, the order parameters for both the oxidized and reduced proteins suggest that local internal motions on the picosecond−nanosecond time scale are small. However, to bolster the change seen in fast motions, the relaxation data for the reduced protein suggest an accompanying change in intermediate time scale motions (microsecond−millisecond) with redox state. Remarkably, the amides requiring exchange terms were, again, not localized to one region but rather spread throughout the protein. These observations are consistent with hydrogen exchange experiments on C102T, which predict a generalized increase in free energy of unfolding for the reduced protein (*14, 18*). Milne et al. (*59*) have suggested that hydrogen exchange behavior can be influenced by the resistance or malleability of the surrounding structure. In the C102T case, the general slowing of hydrogen exchange in the reduced form is apparently linked to the generalized loss of fast (picosecond−nanosecond) and intermediate (microsecond−millisecond) backbone motions. Dynamics measurements have been made on a wide range of time scales and the experimental NMR data in hand suggest a generalized structural difference in dynamics on a range of time scales between the oxidized and reduced forms of yeast iso-1-cytochrome *c*. These NMR results dovetail wth earlier studies based on adiabatic compressibility (*60*), small-angle X-ray scattering (*61*), and amide I infrared spectroscopy (*62*) that also predicted a generalized loss of motion or flexibility in the reduced form of cytochromes *c*.

There is not a strong correlation between the order parameter differences and the redox-dependent changes in average thermal factors (*B*-factors) from crystallographic studies (*4*). Segments 47−59, 65−72, and 81−85 have significantly higher crystallographic thermal factors in the oxidized protein. (*9*) Although we observed decreases in average S^2 values upon oxidation for some residues in these regions, they were not always significant nor were they necessarily coincident with the thermal factor differences. In loop D, for instance, we noted significant decreases in order parameters (a gain of picosecond-nanosecond dynamics) for Tml 72−Thr 78 of loop D linked to oxidation, but the largest *B*-factor changes were noted for Ala 81−Leu 85 in the link between loop D and the C-terminal helix. Residues 83−85 are currently unassigned in the ^{15}N NMR studies presented here, so we were unable to make a direct comparison in this notable region. We observed a loss of picosecond−nanosecond order upon oxidation in the C-terminal helix. In contrast, the average thermal factors in

this region decreased upon oxidation. Last, residues 47−59 in loop C have been implicated as a flexible region in both redox states, based on our ^{15}N relaxation studies. However, we noted a significant increase in order parameters for two of these loop C residues (Tyr 48 and Thr 49) linked to oxidation. The general lack of correlation between order parameters and thermal factors has been noted for other proteins, including staphylococcal nuclease (*51*).

Dynamic Explanations for Results from Previous Mutagenesis Studies. Heteronuclear relaxation studies can detect changes in backbone dynamics, but interpretation of these results in terms of specific structural differences remains difficult in this case, especially since the redox-linked structural changes of iso-1-cytochrome *c* are subtle. A comparison of solid-state and solution structures reveals that the hydrogen bonding of heme propionate 7 changes with redox state (*2*, *7*, *9*). This change displaces the Trp 59 main chain in the crystal structure by about 0.6 Å. Previous ^{13}C NMR work on horse cytochrome *c* showed a significant redox-dependent change at Trp 59 (*63*). The current data show that the order parameter for the Trp 59 amide significantly increases (from 0.78 ± 0.03 to 0.94 ± 0.06) in the reduced form, thus corroborating the crystal structure evidence.

The crystal structures also indicate that the positions of several buried waters are highly dependent on oxidation state. A buried water molecule is linked with positional shifts of the Asn 52, Tyr 67, and Thr 78 side chains in yeast, tuna, horse, and rice cytochromes *c*. These amino acids bracket the stretch of residues (Tml 72−Thr 78) where we observe a continuous, significant gain in order parameters upon reduction. Previously, independent in vivo and in vitro studies (*64*, *65*) have suggested that the evolutionary invariance of both Pro 71 and Pro 76 is due to an important structural change upon redox state of the protein. For instance, replacement of Pro 71 with norvaline leads to complete inactivation of the protein in vitro (*64*). Mutation of Pro 71 to Leu also abolishes function in vivo, while mutation to Val, Thr, Ser, or Ile severely decreased function in vivo (*66*). Mutation of Pro 76 to most any amino acid leads to significant decreases of the protein's functionality in vivo (*65*). The significant increases in order parameters seen upon reduction for Tml 72 to Thr 78 support the contention of a significant change in this region upon change in redox state and suggest that Pro 71 and Pro 76 might act to coordinate that subtle but important redox-dependent conformational change in loop D.

In conclusion, it is interesting to speculate on why significant dynamic differences between the oxidized and reduced states have been observed in this system and in the cytochrome b_5 system. There may be two primary functions of cytochrome *c* that are influenced by protein dynamics: electron transfer and protein−protein interactions. Linking atomic displacement to electron-transfer reorganization energy has proven to be difficult for iso-1-cytochrome *c*. However, these studies suggest that changes in protein dynamics may play a fundamental role in reorganization energy. In addition, the electron transfer function depends on redox partner recognition and docking. Conformational dynamic changes can play an entropically favorable role in protein−protein interactions. Furthermore, despite the fact that cytochromes *c* have multiple protein redox partners, the function that the protein carries out is the same: electron transfer. Thus, a general change in conformational dynamics upon electron transfer may be a common signaling mechanism for interaction of redox partners with various surfaces of cytochrome *c*. The way is now paved to test this suggestion by studying the dynamic properties of variant cytochromes *c* and comparing the results to the extensive in vivo, in vitro, and structural data that have been collected previously.

ACKNOWLEDGMENT

We thank Charles Hauer and Robert Stack of the Wadsworth Center, NYS Department of Health, for performing mass spectroscopic analyses. We thank Lynn McNaughton for assistance with NMR data acquisition and Janet Anderson for programming assistance. We gratefully acknowledge the Wadsworth Center for support and use of the NMR Structural Biology Core.

SUPPORTING INFORMATION AVAILABLE

A table containing amide proton and nitrogen resonance assignments for reduced and oxidized yeast iso-1-cytochrome *c* (C102T) at 25 °C, pH 4.6. This material is available free of charge via the Internet at http://pubs.acs.org.

REFERENCES

1. Moore, G. R., and Pettigrew, G. W. (1990) *Cytochromes c. Evolutionary, structural and physiochemical aspects*, Springer-Verlag, Berlin.
2. Louie, G. V., and Brayer, G. D. (1990) *J. Mol. Biol. 214*, 527−555.
3. Bushnell, G. W., Louie, G. V., and Brayer, G. D. (1990) *J. Mol. Biol. 214*, 585−595.
4. Brayer, G. D., and Murphy, M. E. P. (1996) in *Cytochrome c: a multidisciplinary approach* (Scott, R. A., and Mauk, G., Eds.) pp 103−166, University Science Books, Sausalito, CA.
5. Gao, Y. A., Boyd, J., Pielak, G. J., and Williams, R. J. (1991) *Biochemistry 30*, 1928−1934.
6. Baistrocchi, P., Banci, L., Bertini, I., Turano, P., Bren, K. L., and Gray, H. B. (1996) *Biochemistry 35*, 13788−13796.
7. Banci, L., Bertini, I., Bren, K. L., Gray, H. B., Sompornpisut, P., and Turano, P. (1997) *Biochemistry 36*, 8992−9001.
8. Fetrow, J. S., Cardillo, T. S., and Sherman, F. (1989) *Proteins: Struct., Funct., Genet. 6*, 372−381.
9. Berghuis, A. M., and Brayer, G. D. (1992) *J. Mol. Biol. 223*, 959−976.
10. Mines, G. A., Pascher, T., Lee, S. C., Winkler, J. R., and Gray, H. B. (1996) *Chem. Biol. 3*, 491−497.
11. Cohen, D. S., and Pielak, G. J. (1995) *J. Am. Chem. Soc. 117*, 1675−1677.
12. Bixler, J., Bakker, G., and McLendon, G. (1992) *J. Am. Chem. Soc. 114*, 6338−6939.
13. Nall, B. T. (1996) in *Cytochrome c: a multidisciplinary approach* (Scott, R. A., and Mauk, A. G., Eds.) pp 167−202, University Science Books, Sausalito, CA.
14. Marmorino, J. L., Auld, D. S., Betz, S. F., Doyle, D. F., Young, G. B., and Pielak, G. J. (1993) *Protein Sci. 2*, 1966−74.
15. Gao, Y., Boyd, J., Williams, R. J., and Pielak, G. J. (1990) *Biochemistry 29*, 6994−7003.
16. Betz, S. F., and Pielak, G. J. (1992) *Biochemistry 31*, 12337−12344.
17. Baxter, S. M., Boose, T. L., and Fetrow, J. S. (1997) *J. Am. Chem. Soc. 119*, 9899−9900.
18. Baxter, S. B., and Fetrow, J. S. (1999) *Biochemistry 38*, 4493−4503.
19. Mulligan-Pullyblank, P., Spitzer, J. S., Gilden, B. M., and Fetrow, J. S. (1996) *J. Biol. Chem. 271*, 8633−8645.

20. Cutler, R. L., Pielak, G. J., Mauk, A. G., and Smith, M. (1987) *Protein Eng. 1*, 95−99.
21. Fetrow, J. S., Horner, S. R., Oehrl, W., Schaak, D. L., Boose, T. L., and Burton, R. E. (1997) *Protein Sci. 6*, 197−210.
22. Cohen, D. S., and Pielak, G. J. (1994) *Protein Sci. 3*, 1253−1260.
23. Sherman, F., Stewart, J. W., Parker, J. H., Inhaber, E., Shipman, N. A., Putterman, G. J., Gardisky, R. L., and Margoliash, E. (1968) *J. Biol. Chem. 243*, 5446−56.
24. Piotto, M., Saudek, V., and Sklenar, V. (1992) *J. Biomol. NMR 2*, 661−665.
25. Stone, M. J., Fairbrother, W. J., Palmer, A. G., Reizer, J., Saier, M. H., Jr., and Wright, P. E. (1992) *Biochemistry 31*, 4394−4406.
26. Akke, M., Carr, P. A., and Palmer, A. G. (1994) *J. Magn. Reson. B 104*, 298−302.
27. Abragam, A. (1961) *The principles of nuclear magnetism*, Clarendon Press, Oxford, England.
28. Hiyama, Y., Niu, C., Silverton, J. V., Bavoso, A., and Torchia, D. A. (1988) *J. Am. Chem. Soc. 110*, 2378.
29. Solomon, I., and Bloembergen, N. (1957) *J. Chem. Phys. 25*, 261.
30. Mispelter, J., Momenteau, M., and Lhoste, J. M. (1993) in *NMR of Paramagnetic Molecules* (Berliner, L. J., and Reuben, J., Eds.) pp 299−355, Plenum Press, New York.
31. La Mar, G. N., and de Ropp, J. S. (1993) in *NMR of Paramagnetic Molecules* (Berliner, L. J., and Reuben, J., Eds.) pp 1−78, Plenum Press, New York.
32. Chae, Y. K., and Markley, J. L. (1995) *Biochemistry 34*, 188−193.
33. Lipari, G., and Szabo, A. (1982) *J. Am. Chem. Soc. 104*, 4546.
34. Lipari, G., and Szabo, A. (1982) *J. Am. Chem. Soc. 104*, 4559.
35. Mandel, A. M., Akke, M., and Palmer, A. G. (1995) *J. Mol. Biol. 246*, 144−163.
36. Muchmore, D. C., McIntosh, L. P., Russell, C. B., Anderson, D. E., and Dahlquist, F. W. (1989) *Methods Enzymol. 177*, 44−73.
37. Mossakowska, D. E., and Smith, R. A. G. (1997) in *Protein NMR Techniques* (Reid, D. G., Ed.) Humana Press, Inc., Totowa, NJ.
38. Dumont, M. E., Ernst, J. F., Hampsey, D. M., and Sherman, F. (1987) *EMBO J. 6*, 235−241.
39. Dumont, M. E., Cardillo, T. S., Hayes, M. K., and Sherman, F. (1991) *Mol. Cell. Biol. 11*, 5487−5496.
40. Pollock, W. B., Rosell, F. I., Twitchett, M. B., Dumont, M. E., and Mauk, A. G. (1998) *Biochemistry 37*, 6124−6131.
41. Banci, L., Bertini, I., Cavazza, C., Felli, I. C., and Kouloughliotis, D. (1998) *Biochemistry 37*, 12320−12330.
42. Caffrey, M., Simorre, J. P., Cusanovich, M., and Marion, D. (1995) *FEBS Lett. 368*, 519−522.
43. Gooley, P. R., Caffrey, M. S., Cusanovich, M. A., and MacKenzie, N. E. (1992) *Biochemistry 31*, 443−450.
44. Williamson, M. P., and Asakura, T. (1997) in *Protein NMR Techniques* (Reid, D. G., Ed.) Humana Press, Inc., Totowa, NJ.
45. Qu, K., Vaughn, J. L., Sienkiewicz, A., Scholes, C. P., and Fetrow, J. S. (1997) *Biochemistry 36*, 2884−2897.
46. Farrow, N. A., Zhang, O., Forman-Kay, J. D., and Kay, L. E. (1997) *Biochemistry 36*, 2390−2402.
47. Banci, L. (1993) in *NMR of Paramagnetic Molecules* (Berliner, L. J., and Reuben, J., Eds.) pp 79−111, Plenum Press, New York.
48. Pielak, G. J., Auld, D. S., Betz, S. F., Hilgen-Willis, S. E., and Garcia, L. L. (1996) in *Cytochrome c*: *a multidisciplinary approach* (Scott, R. A., & Mauk, A. G., Eds.) pp 203−284, University Science Books, Sausalito, CA.
49. Farrow, N. A., Muhandiram, R., Singer, A. U., Pascal, S. M., Kay, C. M., Gish, G., Shoelson, S. E., Pawson, T., Forman-Kay, J. D., and Kay, L. E. (1994) *Biochemistry 33*, 5984−6003.
50. Clore, G. M., Driscoll, P. C., Wingfield, P. T., and Gronenborn, A. M. (1990) *Biochemistry 29*, 7387−7401.
51. Kay, L. E., Torchia, D. A., and Bax, A. (1989) *Biochemistry 28*, 8972−8979.
52. Kordel, J., Skelton, N. J., Akke, M., Palmer, A. G., and Chazin, W. J. (1992) *Biochemistry 31*, 4856−4866.
53. Yi, Q., Erman, J. E., and Satterlee, J. D. (1993) *Biochemistry 32*, 10988−10994.
54. Pelletier, H., and Kraut, J. (1992) *Science 258*, 1748−1755.
55. Bai, Y., Sosnick, T. R., Mayne, L., and Englander, S. W. (1995) *Science 269*, 192−197.
56. Akke, M., Skelton, N. J., Kordel, J., Palmer, A. G., and Chazin, W. J. (1993) *Biochemistry 32*, 9832−9844.
57. Nicholson, L. K., Yamazaki, T., Torchia, D. A., Grzesiek, S., Bax, A., Stahl, S. J., Kaufman, J. D., Wingfield, P. T., Lam, P. Y., Jadhav, P. K., and et al. (1995) *Nat. Struct. Biol. 2*, 274−280.
58. Kelly, G. P., Muskett, F. W., and Whitford, D. (1997) *Eur. J. Biochem. 245*, 349−354.
59. Milne, J. S., Mayne, L., Roder, H., Wand, A. J., and Englander, S. W. (1998) *Protein Sci. 7*, 739−745.
60. Eden, D., Matthew, J. B., Rosa, J. J., and Richards, F. M. (1982) *Proc. Natl. Acad. Sci. U.S.A. 79*, 815−819.
61. Trewhella, J., Carlson, V. A. P., Curtis, E. H., and Heidorn, D. B. (1988) *Biochemistry 27*, 1121−1125.
62. Bowler, B. E., May, K., Zaragoza, T., York, P., Dong, A., and Caughey, W. S. (1993) *Biochemistry 32*, 183−190.
63. Turner, D. L., and Williams, R. J. (1993) *Eur. J. Biochem. 211*, 555−562.
64. Wallace, C. J., and Clark-Lewis, I. (1997) *Biochemistry 36*, 14733−14740.
65. Fetrow, J. S., Spitzer, J. S., Gilden, B. M., Mellender, S. J., Begley, T. J., Haas, B. J., and Boose, T. L. (1998) *Biochemistry 37*, 2477−2487.
66. Ernst, J. F., Hampsey, D. M., Stewart, J. W., Rackovsky, S., Goldstein, D., and Sherman, F. (1985) *J. Biol. Chem. 260*, 13225−13236.
67. Bloembergen, N., and Morgan, L. O. (1961) *J. Chem. Phys. 34*, 842−850.

BI9827417